The WIM

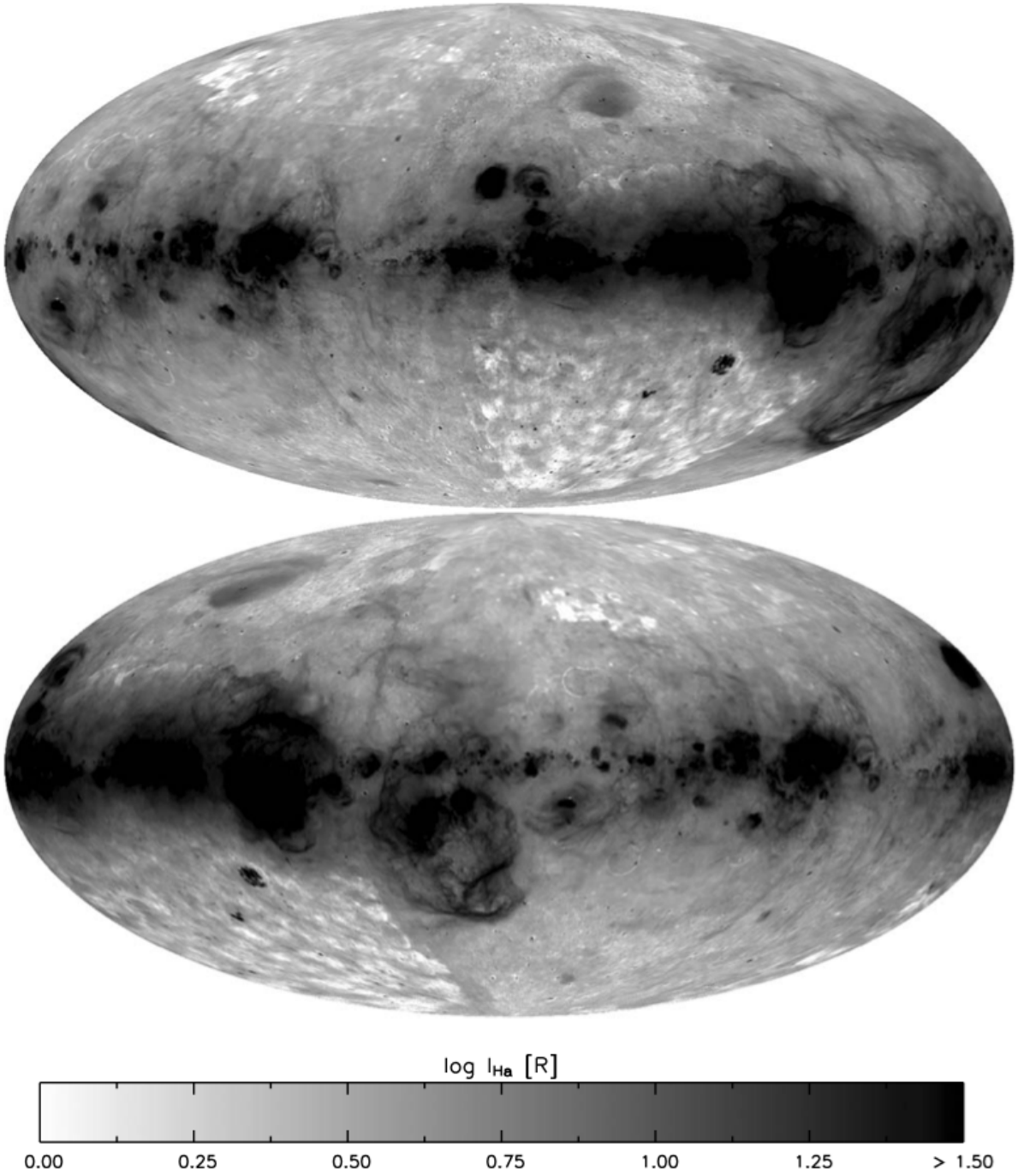

From Haffner et al. (2009), Rev Mod Phys

FIG. 1. Composite all-sky velocity-integrated Hα map. Data from VTSS, SHASSA, and the WHAM northern sky survey (WHAM-NSS) have been combined to produce these very deep (EM $\gtrsim$1 cm^{-6} pc) emission maps. The two Aitoff-Hammer projections are centered at (top) ℓ=0° and (bottom) ℓ=180°. Areas covered by the imaging surveys have arc-minute resolution while those only surveyed by WHAM have one-degree resolution. Emission is predominantly from the Galaxy, although the imaging surveys can contain other bright, extended sources from the local universe ($|v_{\rm LSR}| \lesssim 500$ km s^{-1}; LMC, SMC, M31, etc.). Adapted from Finkbeiner, 2003.

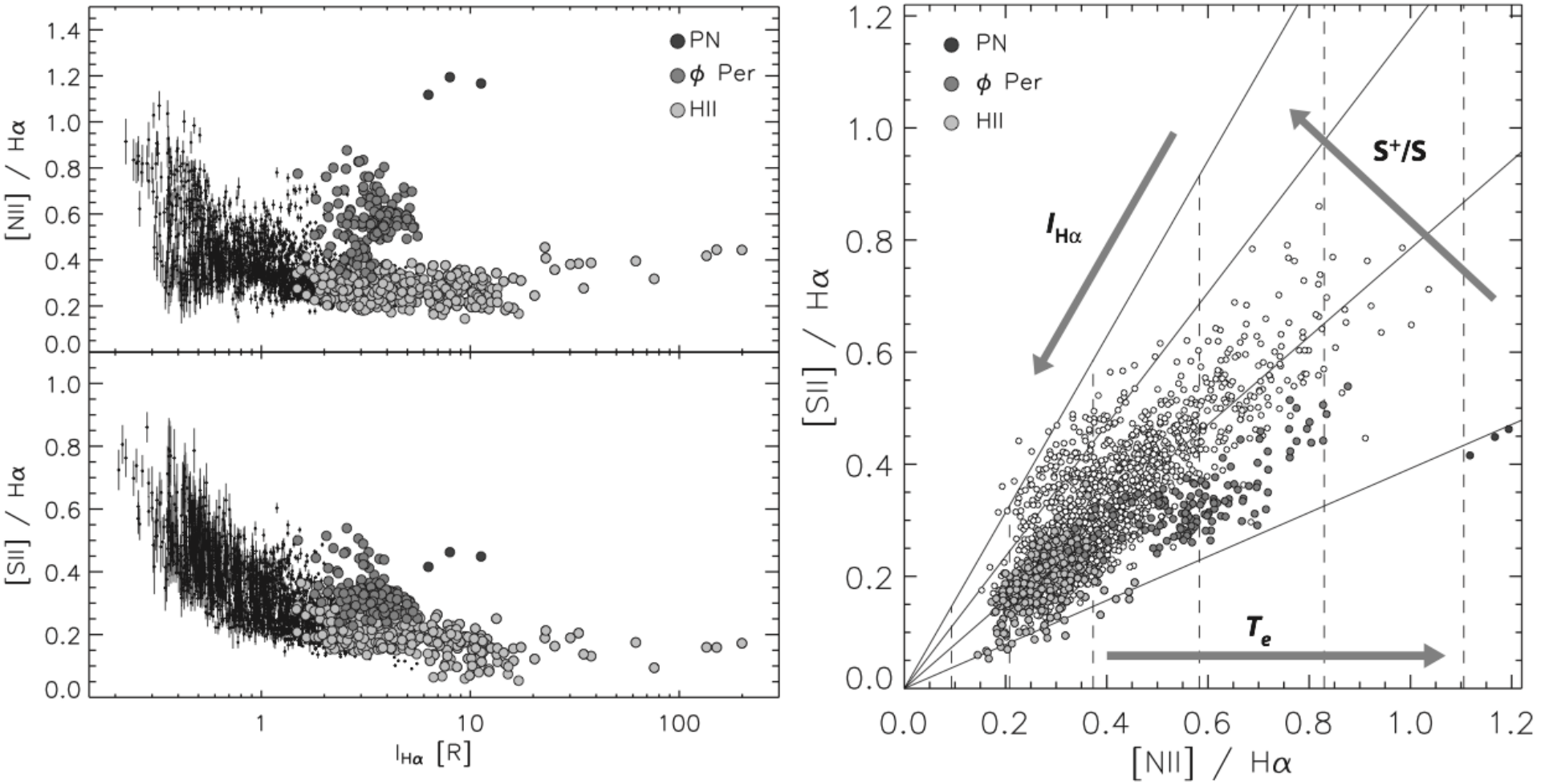

FIG. 2. Diagnostic line ratio diagrams. A large portion of the Galaxy in the direction of the Perseus arm (ℓ=130° to 160° and b=−30° to +30°, approximately) has been surveyed in Hα, [S II], and [N II] with WHAM. These panels show (left) the relationship between the ratios vs the intensity of Hα as well as (right) the relationship between the two ratios for the "local" gas component ($|v_{\rm LSR}|<15$ km s^{-1}). A few specific spatial regions are highlighted with grayscale fill to show the effects of local ionizing sources: the planetary nebula (PN) S216, the H II region surrounding the B0.5+sdO system ϕ Per, and regions near O-star H II regions. Other data points sample the WIM. In the diagram on the right, the vertical dashed lines represent T_e=5000, 6000, 7000, 8000, 9000, and 10 000 K, from left to right. The slanted solid lines represent S$^+$/S=0.25, 0.50, 0.75, and 1.00, lowest to highest slope. These WIM data reveal significant variations in T_e and S$^+$/S from one line of sight to the next. In contrast, classical H II regions all cluster in the lower left corner of this diagram near [N II]/H$\alpha\approx$0.25, [S II]/H$\alpha\approx$0.1. From Madsen, 2004.

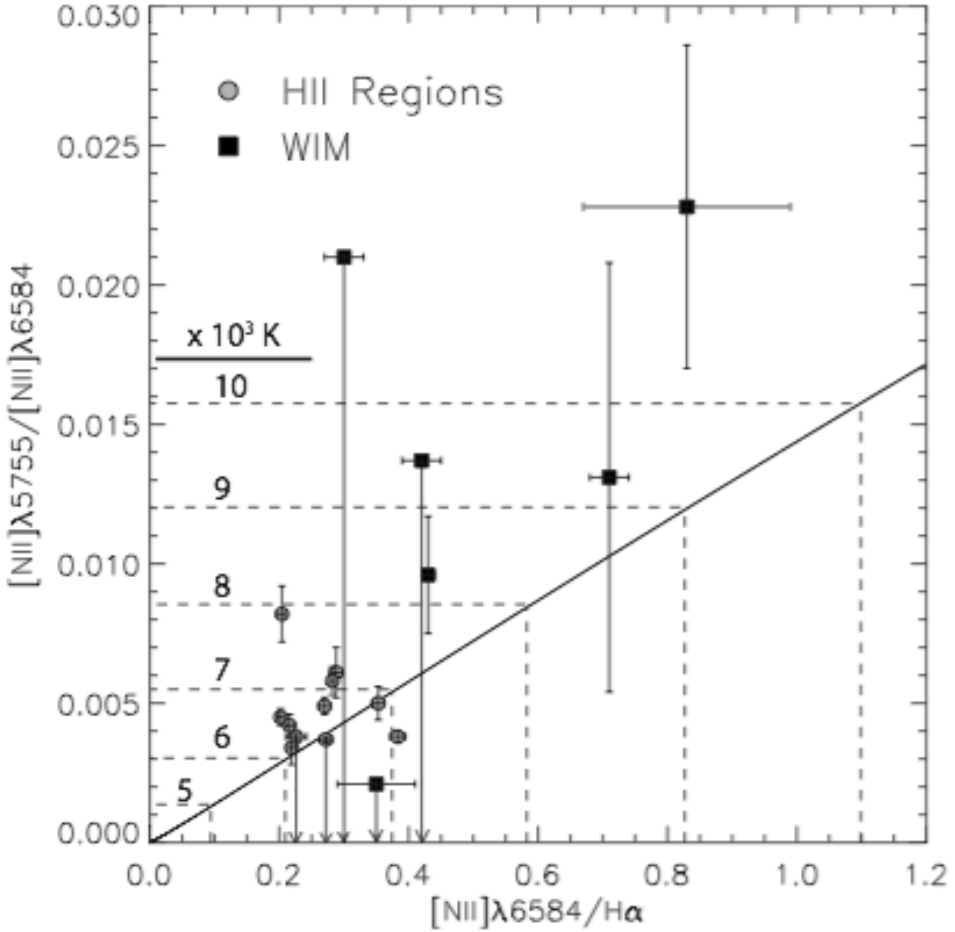

FIG. 3. Elevated temperature in the WIM. Select directions toward (■) brighter diffuse ionized regions show elevated line ratios in both [N II]/Hα and [N II]λ5755/λ6584 compared to (○) H II regions. Dashed lines mark select temperatures derived from each line ratio while the diagonal line traces "unity" in this derived temperature space. WIM directions have higher derived temperatures using either line ratio, but are also systematically above the line of unity, suggesting that measurable temperature inhomogeneities exist along these lines of sight. From Madsen, 2004.

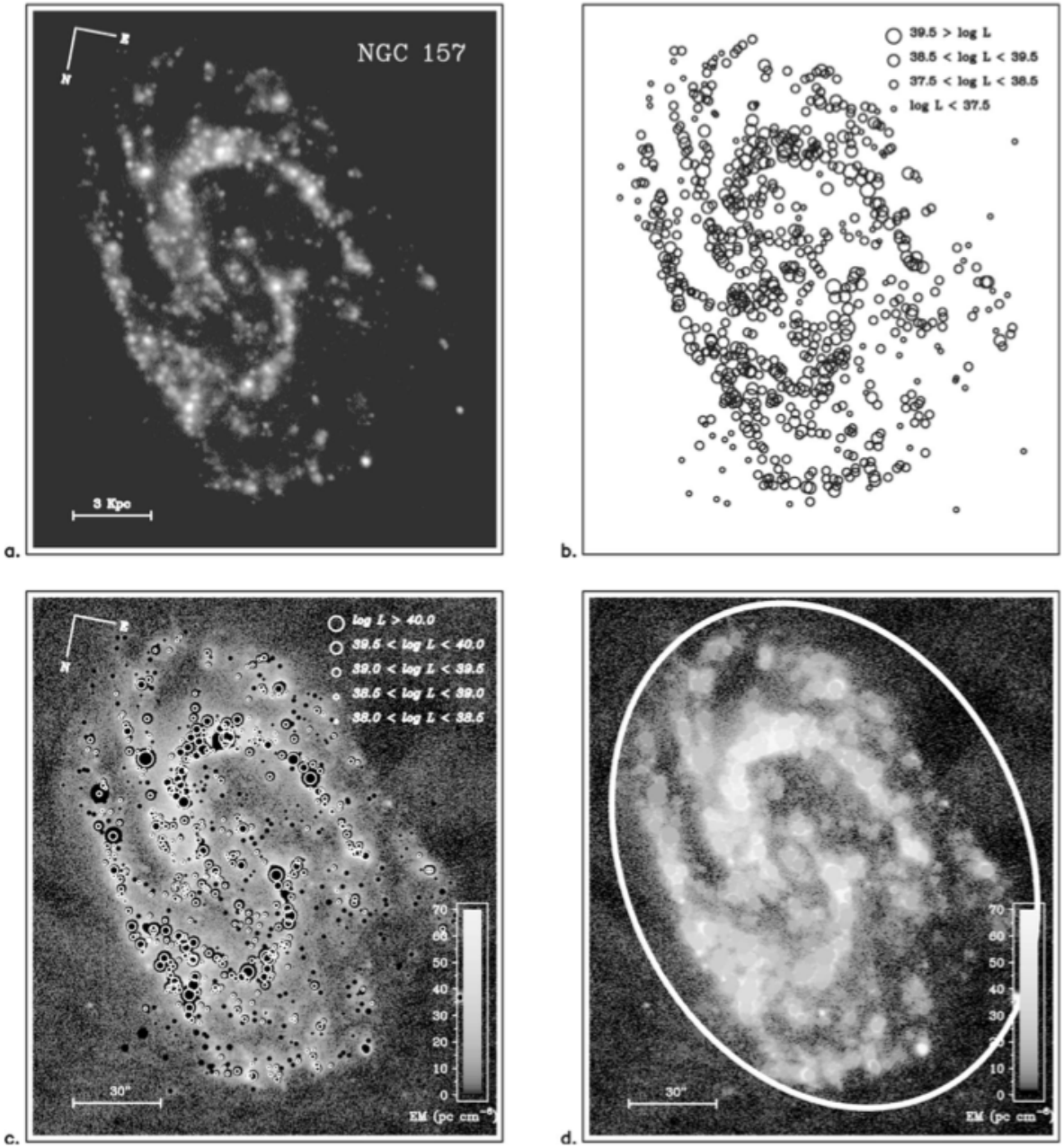

FIG. 9. Steps in the quantification of the total Hα luminosity from the DIG for the representative disk galaxy NGC 157. (a) Continuum subtracted Hα image. (b) Schematic form of H II region catalog, giving position and key to the Hα luminosity of each region. (c) Diffuse Hα map after subtracting off the catalogued H II regions. The brightest H II regions are indicated by circles. (d) Measurement of upper limit for DIG. H II regions are blanked off, then each is assigned a local value of DIG surface brightness. Ellipse shows limit of integrated DIG flux measured. From Zurita *et al.*, 2000.

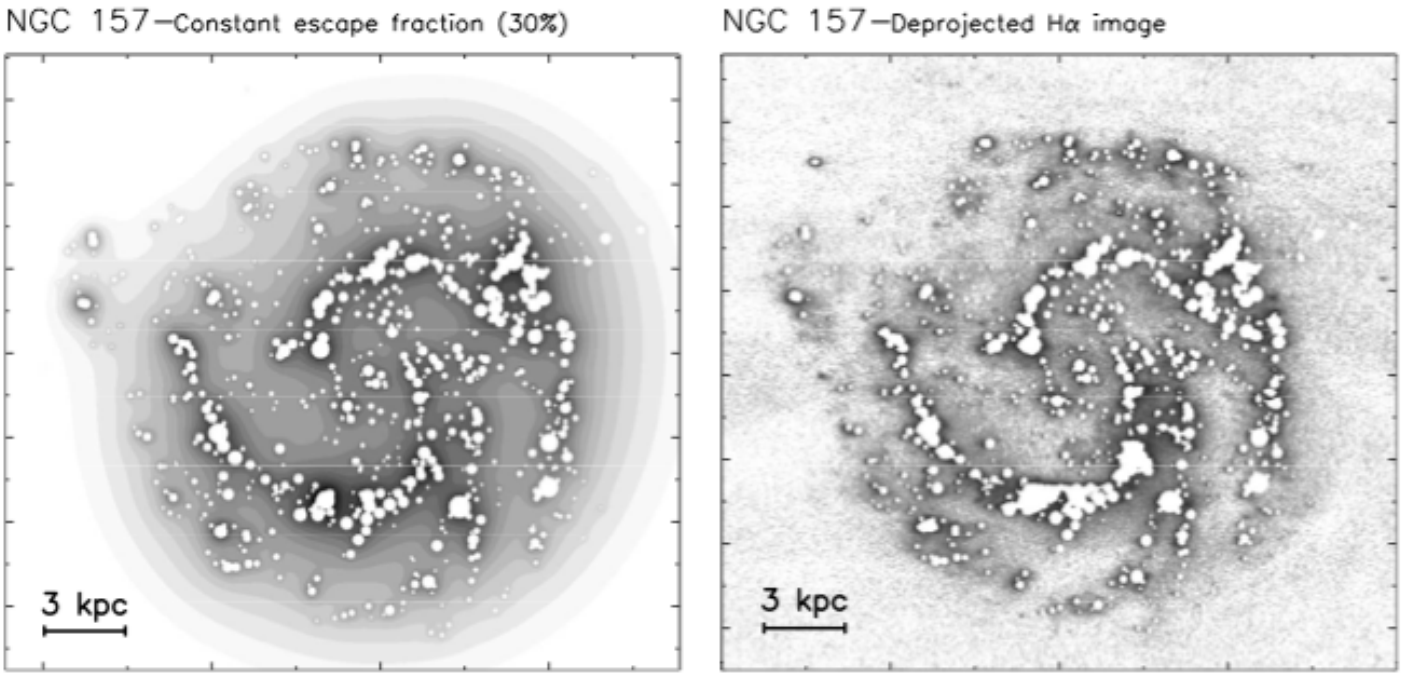

FIG. 12. Comparison of a DIG model with observations. (Left) Modeled surface brightness in Hα of the DIG in the disk of NGC 157 assuming 30% of Lyc photons escape from each H II region, and a simple propagation law through a (macroscopically) uniform slab model for the disk. The result is a projection in the plane of the predicted 3D Hα column density. (Right) Deprojected image of the galaxy with H II regions masked, and a cutoff of $73 \times \cos i$ pc cm^{-6} applied to limit the H II region contamination of the DIG. This shows the basic similarity between these models and the observed DIG, though further refinements are important (see Fig. 13). From Zurita *et al.*, 2002.